Two-body time correlations in (and the structure of) dense krypton gas

P. A. Egelstaff
Physics Department, University of Guelph, Ontario N1G 2W1, Canada

W. Glaser
Technische Universitat, Munchen, Federal Republic of Germany

D. Litchinsky
Aptec Engineering, Ottawa, Canada

E. Schneider
Technische Universitat, Munchen, Federal Republic of Germany

J. B. Suck
Institut Laue-Langevin, Grenoble, France
(Received 27 May 1982)

The van Hove scattering function $S(q,\omega)$ has been measured at 12 state conditions along the 297-K isotherm of krypton gas between 6 and 14×10^{27} atoms/m^3 and for the magnitude of the scattering vectors ($\vec{q}$) between 0.4 and 3.3 Å^{-1}. Integration of the data gives the static structure factors which have a major peak at $q\simeq1.8$ Å^{-1}. These data are compared to Monte Carlo calculations with the use of the pair potential for krypton, and differences due to many-body forces are observed. Then the $S(q,\omega)$ functions are compared to hard-sphere molecular-dynamics simulations and the predictions of the kinetic theory of gases. Data are presented as a function of q for fixed ω, and for low momentum transfer ($q\leq1.8$ Å^{-1}) significant differences are observed, while for higher momentum transfer the hard-sphere results are in reasonable agreement with the data. Diffraction maxima are observed for energy transfers up to 3 meV with the peak position moving to higher q as ω is increased.

INTRODUCTION

The structure and dynamics of dense fluids has made steady advances through the multiple interactions of neutron scattering studies, computer simulation work, and basic theory. Natural complexities in this field have often prevented progress until this three-pronged approach could be focused onto the problems.

With the advent of a new, versatile, and powerful neutron spectrometer [the I.N.4 instrument at the Institut Laue-Langevin (ILL)] it has become possible to measure the static and dynamic structure factors systematically through the phase diagram. We have chosen to work along the room-temperature isotherm of krypton, studying 12 states with densities between 6 and 14×10^{27} atoms/m^3 (i.e., from approximately the critical density to 80% of the triple-point liquid density). These data, when compared to simulation studies and theoretical results, allow effects due to many-body forces and many-body collisions to be explored in a systematic way. In particular, we have extended the earlier structural studies[1,2] to twice the density, that is, into the range where higher-order forces might influence the structure. Also, we have measured the dynamic structure factor in a density range well beyond the binary collision dominated regime and also for a system for which the time-dependent pair correlation function can be observed. This work extends beyond other investigations[3–5] which have covered low momentum transfers, incoherent (single-particle) scattering, or a restricted density regime.

In the next two sections we describe the experiment (see Table I) and the data analysis. Then we present the data for the minimum and maximum densities for the first half of the experiment, namely, 10.6 and 13.8×10^{27} atoms/m^2 at $T=297$ K (since the complete data set is too large to be covered in one paper). These data are compared to computer simulation and theoretical results in a later section.

TABLE I. Summary of experimental conditions. N7 is 25-mm internal diameter. N8 is 38-mm internal diameter.

Vessel	Run no.	Pressure (10^5 Pa)	Density (10^{27} atoms/m^3)	Temperature (°C)
N7	940[a]	942	13.84	23.7
N7	942	800	13.25	23.8
N7	944	670	12.59	23.8
N7	947	568	11.95	24.0
N7	949	486	11.31	24.0
N7	951[a]	415	10.63	24.1
N8	959	421	10.76	24.5
N8	961	372	10.13	24.5
N8	963	322	9.42	24.5
N8	965	370	10.11	24.7
N8	967	323	9.44	24.7
N8	969	278	8.64	24.8
N8	971	240	7.79	24.8
N8	973	216	7.15	24.9
N8	976	181	6.06	25.0

[a]Runs reported here.

EXPERIMENTAL DETAILS

Krypton gas of high purity was held in cylindrical pressure vessels. The pressure was raised by a cryopumping system from low-pressure supply cylinders, and pressures were determined by calibrated Bourdon gauges. Two vessels made of aluminum alloy were used, one with internal and external diameters of 25 and 43 mm, respectively, was used for pressures from 940 to 400×10^5 Pa, while another with internal and external diameters of 38 and 50 mm, respectively, was used for pressures between 420 and 180×10^5 Pa. The vessels were designed so that the change of diameter over this pressure range was only 0.07%. The ends of each vessel were screened by cadmium sheet, and a cadmium diaphragm attached to the vessel reduced the neutron beam height to the internal cylinder diameter. The exposed cylinder length (10 cm) exceeded the beam width, and the cylinder axis was horizontal.

Neutron time-of-flight spectra were taken on the I.N.4 spectrometer at the ILL high-flux reactor. Data were taken at the highest pressure, and then gas was released into a reservoir in stages reducing the density in a number of steps of about 6% each. Finally, the gas was cryopumped back into the supply cylinder leaving the vessel empty. A typical measurement took about 20 h, and pressures were stable to $\sim1.5\times10^5$ Pa and temperatures to 0.2 °C over this period. Data were also taken on vanadium samples constructed as spirals to simulate each gas sample. Immediately before and after each series of measurements on a pressure vessel, the appropriate vanadium sample was measured and a background recorded with an empty (vanadium) holder in the sample position. These measurements served as a calibration and a measure of instrumental stability. The vanadium samples had cadmium diaphragms attached to them at the same points as the corresponding pressure cells, and each could be positioned accurately and reproducibly. The neutron beam was 4 cm high (vertical) and 8.5 cm long (horizontal).

The neutron spectrometer is a phased rotating crystal spectrometer using two graphite crystals; data were recorded into 512 time channels, each of 12.5 μsec. It was operated at a wavelength $\lambda=2.54$ Å, and 210 ^{3}He counters (each 2.5-cm diameter) were placed at 4.03 m from the sample in a vertical arc extending over an angular range of 8° to 85°. This arrangement allowed a range of the elastic scattering vector from 0.4 to 3.3 Å^{-1} to be covered (with good angular resolution) at one set of instrumental settings. These settings were not changed for the three-week duration of this experiment. The full width at half maximum of the resolution function (determined from the elastic scattering of vanadium) was 0.85 meV (so that an energy transfer of 1 meV is 2.4 resolution widths).

Measurements were made with both pressure vessels at a common pressure to test for consistency: this test was satisfactory. In addition, for the 38-mm diameter vessel, measurements were repeated at two pressures by repressurizing the vessel *in situ* as a further consistency test which was satisfactory also. These tests confirmed the stability of the spectrome-

ter and the gas handling equipment. A complete list of the experiments is given in Table I.

DATA CORRECTIONS FOR ABSORPTION AND MULTIPLE SCATTERING

The absorption factors were calculated for each time channel using a modified version of an ILL program.[6] In this modified program a cross section of the sample, including the container and other environmental parts, was divided into a narrow grid of scattering points. This allowed not only the neutron velocities before and after scattering to be taken into account but also the realistic scattering geometry due to shielding of parts of the sample environment.

The raw data are the sum of singly and multiply scattered neutrons by the container and the gas sample, and the multiply scattered component may be removed by calculation. To do this we employed a Monte Carlo simulation of the experiment using a program written by Copley.[7] The efficiency of this program was low, especially for elastic multiple scattering. The program was improved by treating the real detector geometry and by exact calculation of the fractions of Debye-Scherer cones passing through detectors.[8] In this way the subroutine for elastic scattering was made almost two orders of magnitude faster, and the total computing time for multiple scattering calculations was reduced by a factor of 3, which is a substantial saving if large numbers of neutron fates have to be calculated. In these Monte Carlo simulations the (symmetrized) dynamic structure factor for the gas was approximated by the formula

$$\hat{S}(q,\omega)=\frac{S(q)}{\sqrt{2\pi}\,\sigma}\exp\left[-\frac{\omega^2}{2\sigma^2}\right] \tag{1}$$

with

$$\sigma^2=\frac{kT}{MS(q)}q^2 ,$$

where $\hbar q$ and $\hbar\omega$ are the momentum and energy transferred in the scattering event. The pressure vessel was represented by a container of pure perfectly polycrystalline aluminum. For each detector angle and a time-of-flight range of 50 channels of 25 μsec each, 5×10^4 neutron fates were simulated both for the empty container and the sample plus container run. This took about 40 min on a CDC CYBER-175 computer. Only 20 angles were simulated, and data for the other angles were deduced by a linear interpolation.

These results showed a central peak of (mainly) multiple Bragg scattering, but the statistical precision was unsatisfactory. To improve this we averaged this central region over all angles to give the shape of the multiple Bragg component. This shape was found to be equal to the resolution function, but its centroid was slightly shifted in time (by 0.7 channels) to correspond to the average flight path for multiply scattered neutrons. Therefore we decided to use this shape for the central ten channels and to equate its area to the corresponding area determined at each angle in the Monte Carlo runs. For the remaining (40) channels we used the Monte Carlo data directly. Data analyzed in this way are used in Figs. 5–8. Data from the multiple scattering simulation are shown in Fig. 1, or subtracted directly in Fig. 4.

These results were compared to the sample experimental results, which had been normalized to an absolute scale with the use of the vanadium experimental results. It was found that for low and medium angles the calculated multiple scattering cross sections (without adjustments) were in excellent agreement with measured data at energy transfers greater than about 4 meV (Fig. 1). However at high angles the range of 50×25-μsec channels was not large enough. The range was extended to 100×25-μsec channels through the assumption that for large time shifts the multiple scattering is isotropic. In this case the multiple scattering for large time shifts may be read off the low-angle data, and angles of 8.25°, 9.0°, and 9.75° were used for this purpose. Figures 1(a)–1(d) show the normalized experimental data and multiple scattering results for a low and a medium angle; note the poor statistical accuracy of the simulation.

With these results the data were reduced with the use of the following formula:

$$\frac{\sigma_s}{4\pi}\frac{k}{k'}f(k')\hat{S}(\theta,\omega)e^{-\hbar\omega/2kT}=\frac{I_{SC}(\theta,\omega)}{A_{SSC}(\theta,\omega)}-\frac{A_{CSC}(\theta,\omega)I_C(\theta,\omega)}{A_{SSC}(\theta,\omega)A_{CC}(\theta,\omega)}-\Delta_m(\theta,\omega) , \tag{2}$$

where

$$I_{SC}(\theta,\omega)=I_{SCE}(\theta,\omega)-A_{ESC}I_E(\theta,\omega) ,$$

$$I_C(\theta,\omega)=I_{CE}(\theta,\omega)-A_{EC}I_E(\theta,\omega) ,$$

where $f(k')$ is the detector efficiency for wave number k', the $I(\theta,\omega)$ are properly normalized and time to energy transformed scattering intensities per channel, the $A(\theta,\omega)$'s are the absorption factors (S, C, and E mean sample, container, and empty environment) which were calculated for each time channel with the appropriate absorption cross sec-

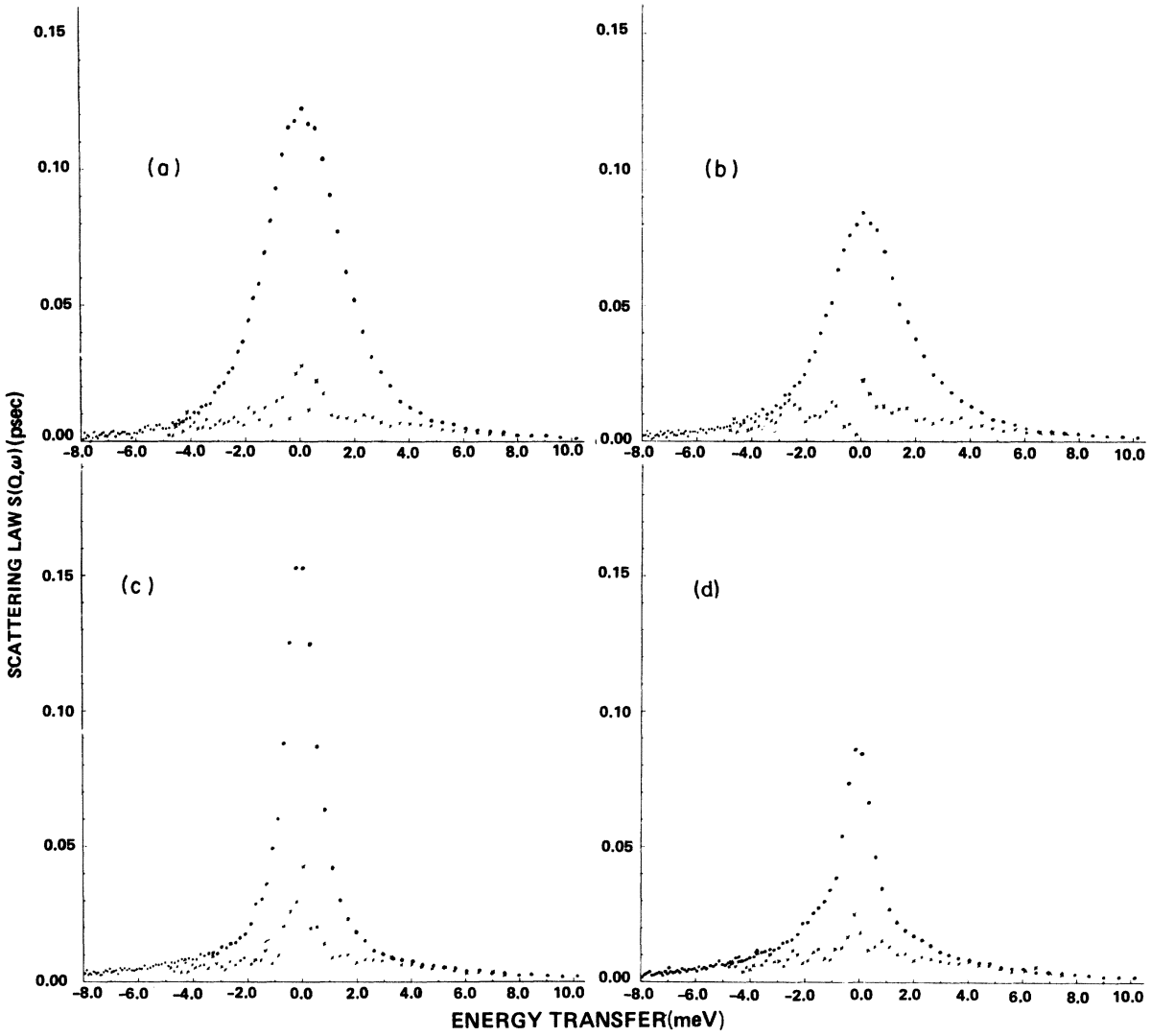

FIG. 1. Examples of experimental data (solid circles) and the Monte Carlo simulation of the multiple scattering (crosses). (a),(b) Normalized intensity and multiple scattering data for $\theta=29.8°$. (a) $\rho=10.6\times10^{27}$ atoms/m.^{3} (b) $\rho=13.8\times10^{27}$ atoms/m^3. (c),(d) Normalized intensity and multiple scattering data for $\theta=9°$. (c) $\rho=10.6\times10^{27}$ atoms/m.^{3} (d) $\rho=13.8\times10^{27}$ atoms/m^3. Note the large statistical fluctuations on the Monte Carlo data.

tion. $\Delta_m(\theta,\omega)$ is the multiple scattering correction, evaluated from the absorption corrected results of sample plus container and empty container Monte Carlo runs. Energy transfers are assumed to be positive when the neutron gains energy.

The function $\hat{S}(\theta,\omega)$ obtained from Eq. (2) is the symmetrized scattering law and will be interpreted in several different ways in the following sections. Although q is a function of (θ,ω), its variation for $\theta=$const is small because of the relatively high mass of krypton. Over our range (see Fig. 4) it is sufficient to use the approximation

$$q=q_{\rm el}\left[1+\frac{\hbar\omega}{4E_0}\right], \tag{3}$$

where $q_{\rm el}$ is the value for $\omega=0$, and E_0 is the incident energy. This expression gives a q variation of 2% per meV.

STATIC STRUCTURE FACTOR: RESULTS AND DISCUSSION

The reduced data were summed over all time-of-flight channels to give the intensity as a function of

angle. Statistical errors are ~0.1% and are less significant than the systematic errors arising from corrections discussed above. A small correction[9] (~1%) was made to these intensities to compensate for Doppler shifts (often called a Placzek correction). A small correction (~2.5%) was also made for incoherent scattering using the cross section data in Ref. 1.

It is of interest to compare these results to a Monte Carlo simulation[2] using the pair potential for krypton due to Barker *et al.*[10] This comparison is shown in Fig. 2 for the six densities in the first half of the experiment, and significant differences can be seen. It should be noted that no scale factor adjustments were made in these diagrams, and the overall agreement indicates that the systematic error is small. Simulations[2] using the Axilrod-Teller triple dipole potential in addition to the pair potential suggested that the effect of this term was small and decreased with increasing density. This has been confirmed in a recent study[11] at higher densities. Therefore the discrepancies seen in Fig. 2 must be due to either or both the shorter-ranged three-body forces and the many-body forces. It is clear that all these terms change the shape of $S(q)$ continuously with density, and that (by comparison to the data of Ref. 1) the visible differences from the pair potential calculations extend over a greater range of q as the density is raised. Simulations using models for many-body forces are required to improve this interpretation.

It should be noted that these conclusions differ from those usually drawn[12] from the structure of liquid argon. However, in that case, comparisons are made with an effective pair potential and so are inconclusive. Also the higher density at the triple point may have reduced the observable effects.[11]

DYNAMIC STRUCTURE FACTOR: RESULTS AND DISCUSSION

At this stage of the evaluation the data taken at each state of krypton consist of 62 spectra, and each spectrum is represented by 100 points. There is some redundancy since energy gain and loss processes are related by the detailed balance factor. Even so the quantity of data is too large for it to be presented completely. Therefore we shall present a condensation of the data at two states only and publish the other states in a later paper.

Molecular-dynamics (MD) calculations have been made for the hard-sphere fluid by Yip *et al.*[13] for three states. The middle member of these states corresponds to our state at a density of 10.6×10^{27} atoms/m^3, if a hard-sphere diameter of 3.53 Å is used. This diameter was chosen to give a reasonable

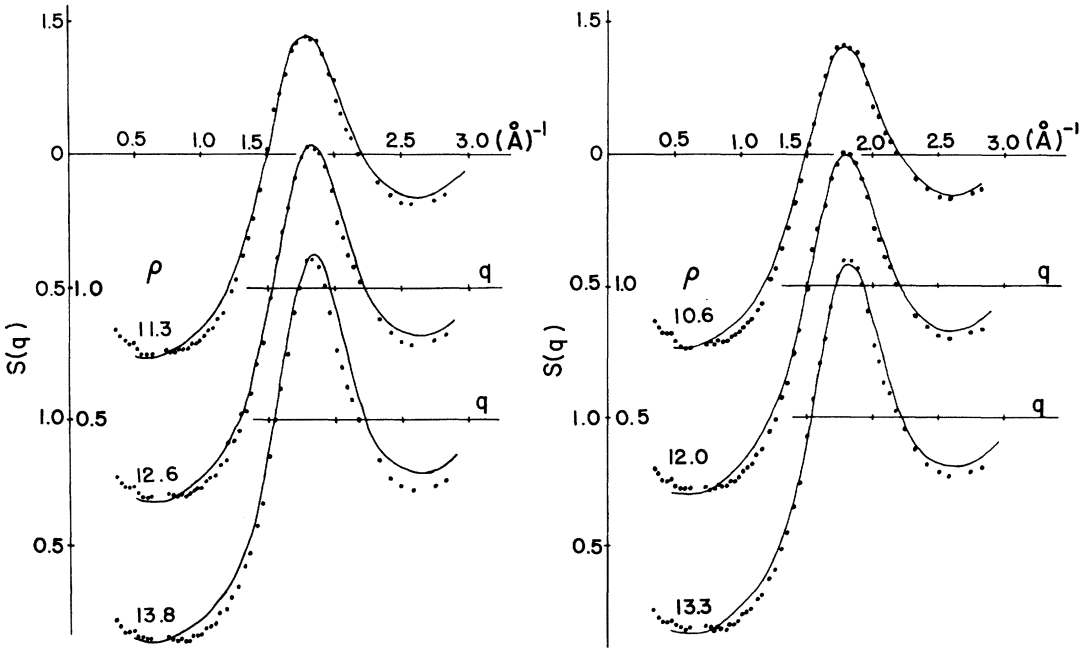

FIG. 2. Comparison of the structure factor obtained in a Monte Carlo simulation[2] using the krypton potential (solid line) with the experimental results (circles) at densities (in units of 10^{27} atoms/m^3) shown on the figure. There are no adjustment factors in this comparison.

fit between the hard-sphere structure factor and the experimental $S(q)$, as shown in Fig. 3, and may be compared to 3.59 Å at $u(r)=0$ for the Barker *et al.*[10] potential. A comparison between five spectra and the hard-sphere simulation is shown in Fig. 4. These cases were chosen to illustrate that at low angles krypton gas spectra are taller than the simulation while at angles near 30° the reverse is true, and at higher angles there is little difference. This conclusion may be illustrated by a comparison of the full widths at half maximum amplitude. These are shown in Fig. 5 as a function of q for the experimental results (crosses) at $\rho=10.7\times10^{27}$ atoms/m^3 after correcting for resolution, and the hard-sphere kinetic theory (full line) of Dufty *et al.*[14] which is in fair agreement with the hard-sphere (circles) simulations.[13] Also shown is the perfect gas result (dashed line), and it is seen that the experimental results accidentally follow the perfect gas from 0.35 to 1 Å^{-1} (see below), and then move over to the hard-sphere line which is followed approximately from 1.8 to 3.3 Å^{-1}. Figure 6 shows a similar plot for the data at $\rho=13.8\times10^{27}$ atoms/m^3, and in this case the widths are always less than the perfect gas values. They differ significantly from the hard-sphere data for $q<1.2$ Å^{-1} where they are density dependent, being less than the perfect gas at this density, about equal in Fig. 5, and greater at low density, where

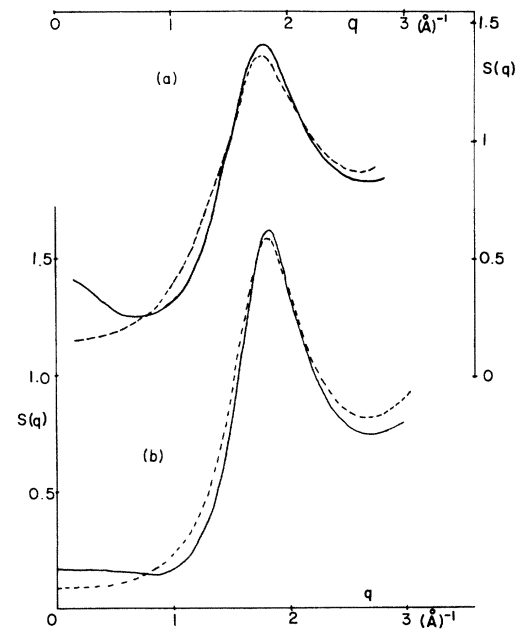

FIG. 3. Comparison of hard-sphere structure factor (dashed line) with two of the experimental results of Fig. 2 (solid line). (a) $\rho=10.6\times10^{27}$ atoms/m.^{3} (b) $\rho=13.8\times10^{27}$ atoms/m^3. A single hard-sphere diameter of 3.53 Å was chosen to fit the peak positions.

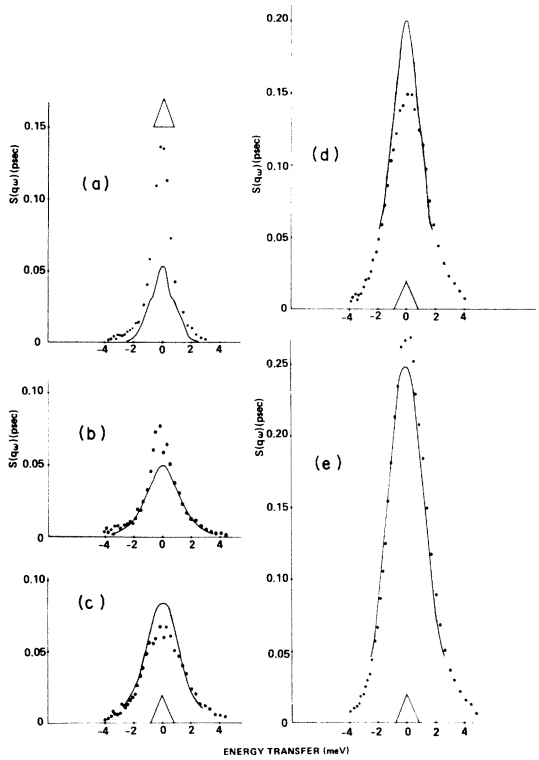

FIG. 4. Comparison of the spectra of inelastically scattered neutrons (solid circles) from krypton gas at $\rho=10.6\times10^{27}$ atoms/m^3 with the hard-sphere MD simulations[12] (solid lines). Five angles are chosen to correspond to the momenta q of the simulations: (a) $\theta=8.25°$, (b) $\theta=16.5°$, (c) $\theta=24.7°$, (d) $\theta=33.2°$, and (e) $\theta=41.1°$; the triangles show the resolution width. The values of q for elastic scattering are 0.35, 0.70, 1.05, 1.40, and 1.74 Å^{-1}, respectively.

they are close to the hard-sphere data. But for $q>1.8$ Å^{-1} the observed widths are close to the hard-sphere widths, and the agreement is similar to that observed for the lower density. Thus if the wavelength of a Fourier component is less than the interparticle spacing the collisions appear to be similar to hard-sphere collisions.

The experimental spectra extend to an energy transfer of about ±5 meV and may be plotted naturally as a function of q for fixed ω. This is a convenient way to compare theory to experiment; since data from all angles may be combined in one figure, the redundancy of $\pm\omega$ values is removed, and the spectra may be represented by a small number of suitably chosen ω values. For this purpose we chose $|\hbar\omega|$ values of 0, 1, 2, and 3 meV, and the magnitudes of $\hat{S}(\theta,\omega)$ at these points were read from smoothed spectra. Using the exact q values for each (θ,ω) a $\hat{S}(q,\omega)$ table was prepared and $\pm\omega$ data for the same q were averaged. The $\pm\omega$ results were in

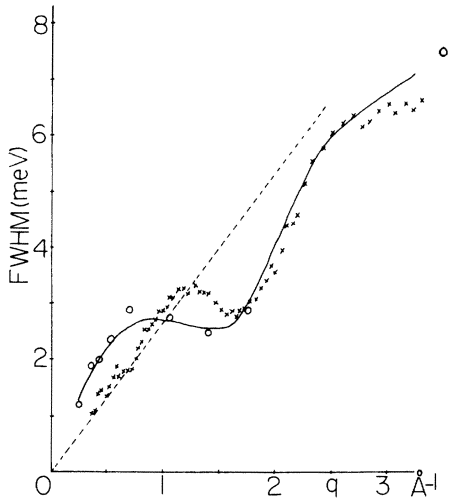

FIG. 5. Full widths at half maximum amplitude in $S(q,\omega)$ for $\rho=10.6\times10^{27}$ atoms/m^3. Solid line, kinetic theory of hard spheres[14]; dashed line, perfect gas; circles, hard-sphere MD data[13]; crosses, krypton experiment corrected for resolution.

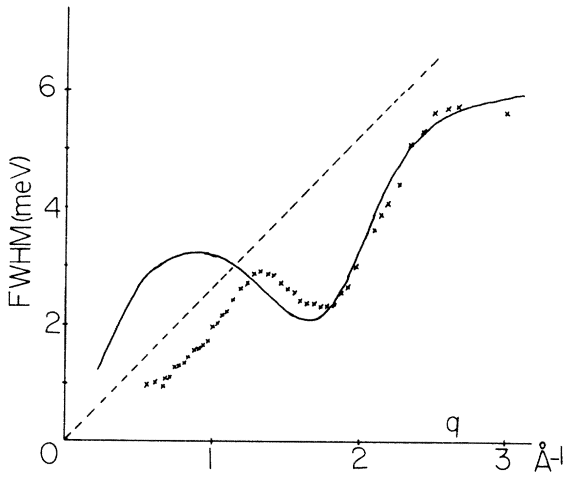

FIG. 6. Same as Fig. 5 but for $\rho=13.8\times10^{27}$ atoms/m^3. No hard-sphere simulations are available for this density.

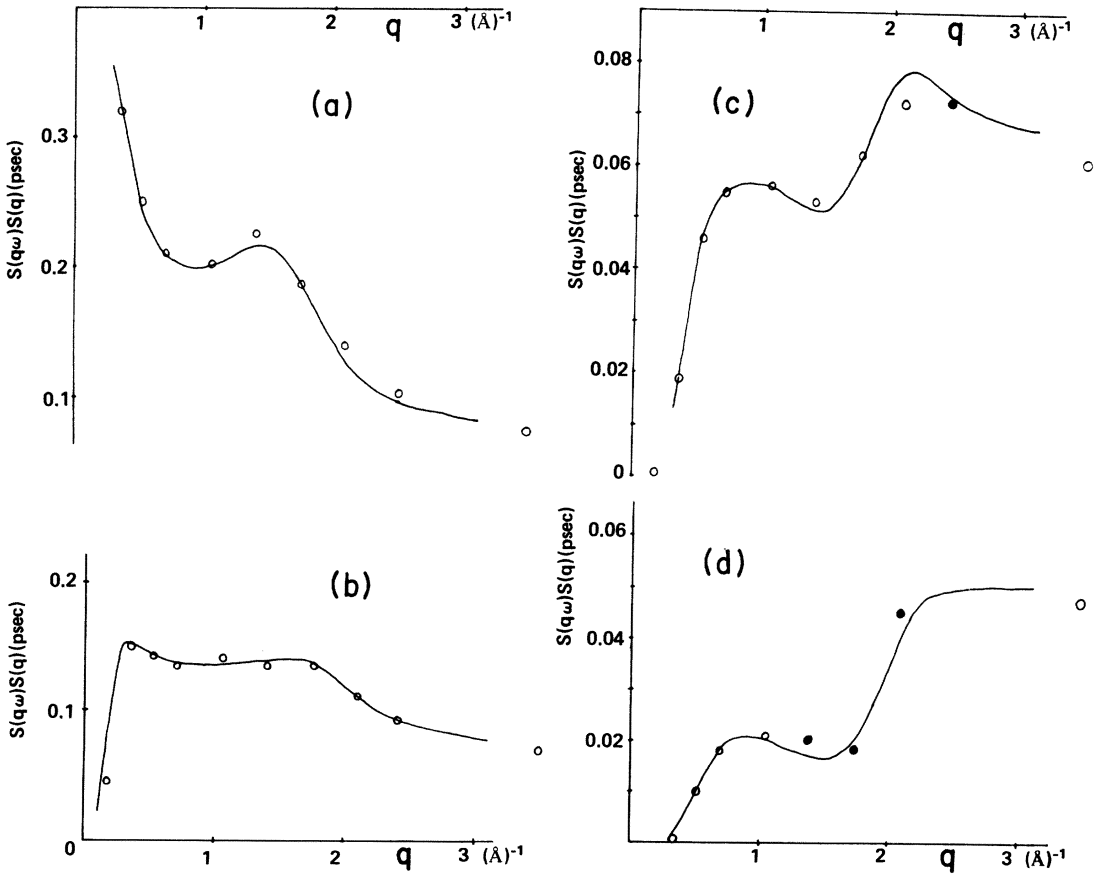

FIG. 7. Scattering law for the hard-sphere fluid at a density of 10.6×10^{27} spheres/m^3 with $\sigma=3.53$ Å. The circles are the MD simulations of Yip *et al.*[13] (shaded circles are data obtained by extrapolation from tables provided by Yip *et al.*), and the lines are calculations provided by Dufty *et al.*[14]

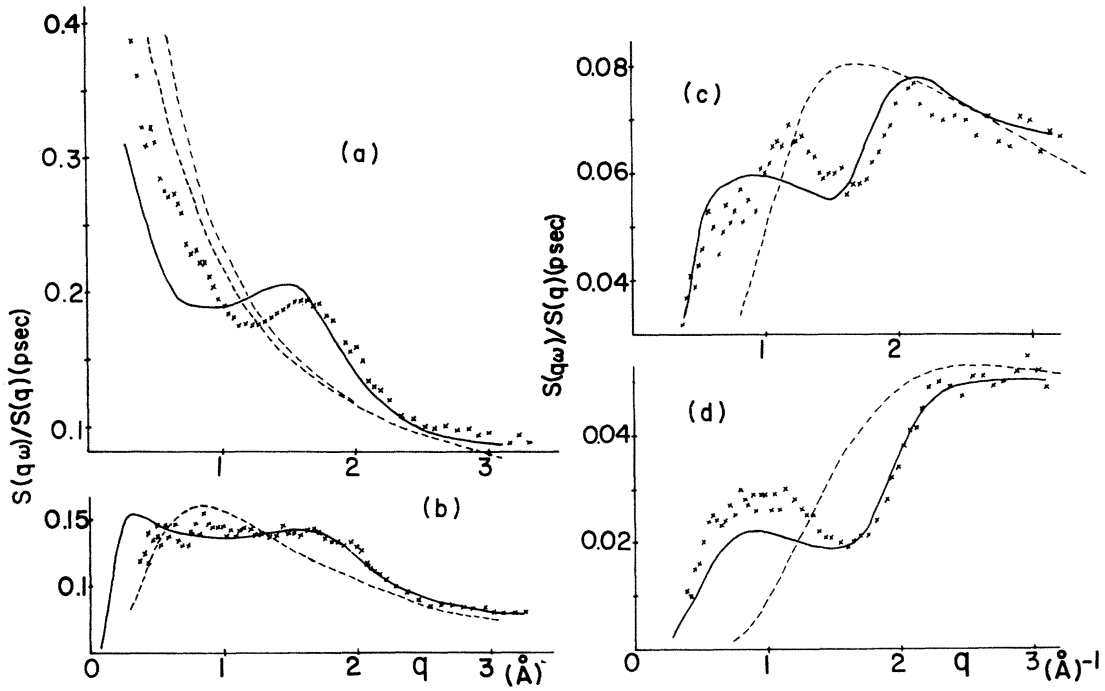

FIG. 8. Scattering law for dense krypton gas compared to the hard-sphere fluid. Diagrams for energy transfers of 0, 1, 2, and 3 meV are shown as (a)—(d), respectively. The density is 10.6×10^{27} atoms/m^3, and the temperature is 297 K; crosses, experimental data; solid line, kinetic theory including resolution broadening; dashed lines, perfect gas. The upper and lower dashed lines in (a) are unbroadened and broadened by the resolution function, respectively; other dashed lines include resolution broadening, which is a smaller effect than in (a). No adjustment factors have been included in either the experimental or the theoretical data.

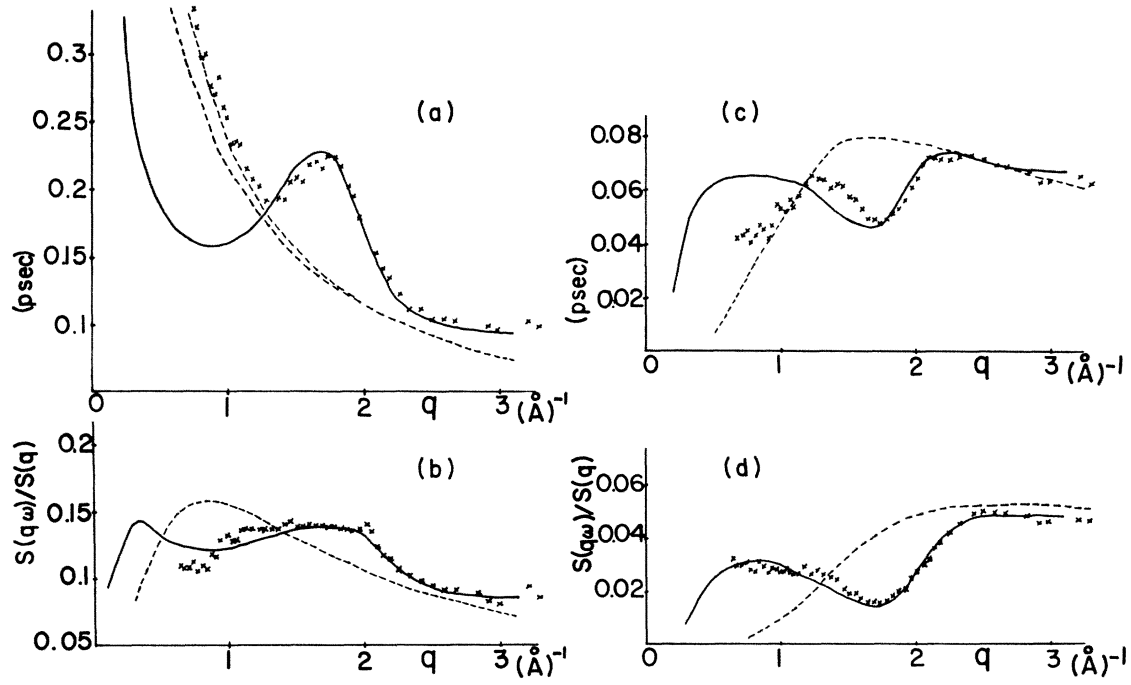

FIG. 9. Same as Fig. 7 except that $\rho=13.8\times10^{27}$ atoms/m^3.

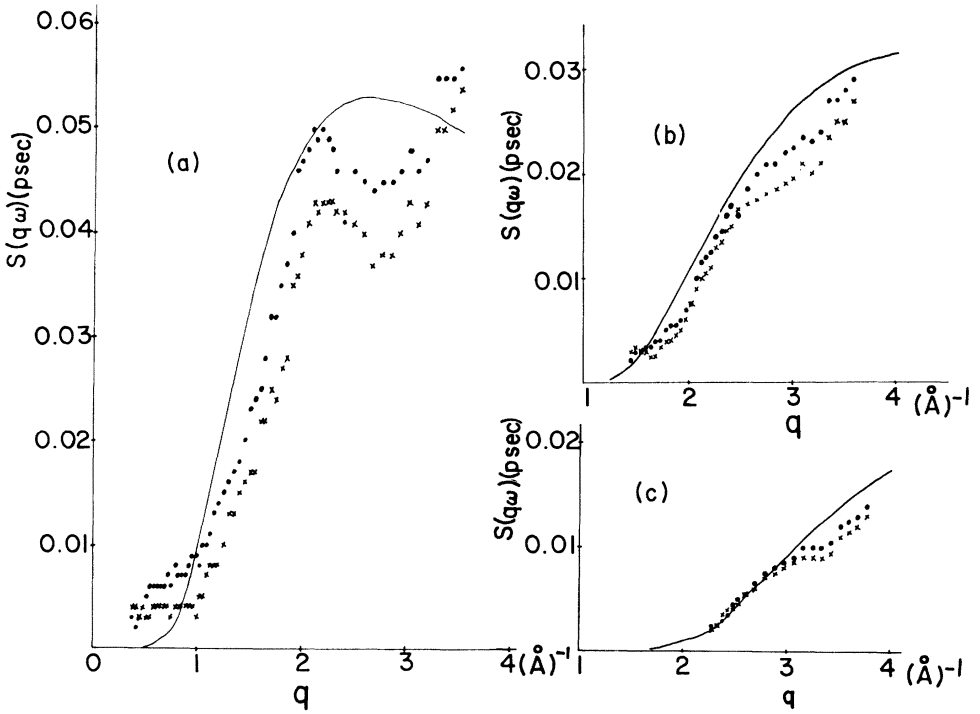

FIG. 10. Scattering law for dense krypton gas at $\hbar\omega = 3$, 5, and 7 meV shown as (a), (b), and (c), respectively. Circles, $\rho = 10.6 \times 10^{27}$ atoms/m^3; crosses, $\rho = 13.8 \times 10^{27}$ atoms/m^3; solid line, the perfect gas including resolution broadening.

agreement within the statistical fluctuations. The value of $S(q)$ at each of these q's was taken from the table of $S(q)$ data by interpolation between neighboring points, and the ratios $\hat{S}(q,\omega)/S(q)$ evaluated. Groome *et al.*[15] point out that this ratio is simply related to the resolvant operator appearing in the generalized Enskog equation and so is an appropriate point at which to make contact with kinetic theory.

The hard-sphere kinetic-theory calculations of Dufty *et al.*[14] are shown in this form in Fig. 7 compared to the molecular dynamics simulation of Yip *et al.*[13] It can be seen that there is generally good agreement, although the error on the MD data is not known to us. Consequently, it would appear to be reasonable to use the calculations of Dufty *et al.*[14] in regions of (ω,q,ρ) space not covered by the MD simulation, and this is done in later figures. Dufty *et al.*[14] have folded their theoretical predictions with our (vanadium) resolution function so that direct comparisons with experimental results may be made. Because the width (0.85 meV) for elastic scattering by vanadium is small compared to the widths in Figs. 5 and 6 this correction is not very significant, but it is worthwhile making this adjustment. We show in Figs. 8(a)—8(d) and 9(a)—9(d) these data for $\hbar\omega = 0$, 1, 2, and 3 meV, compared to the predictions. The experimental errors vary with (q,ω), and the data fluctuations show the variation of the random errors. The systematic errors are comparable to or less than the random errors as shown in the discussion of Figs. 2 and 10. For $\hbar\omega = 0$ the relationship between theoretical and experimental results may be inferred from the widths at half height (Figs. 5 and 6). For energy transfers of 1 meV the hard-sphere data and the krypton data show a weak oscillation corresponding to the peak in $S(q)$, but at 2 and 3 meV a dip occurs near this position. The discrepancy between the hard-sphere results and this experiment is seen (Figs. 4 and 8 or 9) to be largest for small energy transfers or $\hbar\omega < 1$

TABLE II. Positions of interference maxima as a function of $|\hbar\omega|$.

$\lvert\hbar\omega\rvert$ (meV)	q_{max} (Å^{-1}) $\rho = 10.6$	$\rho = 13.8$
0	1.73	1.78
1	1.76	1.82
2	1.95	1.95
3	2.2	2.2
5	~2.6	~2.6
7	~3.2	~3.2
$S(q)$	1.79	1.82

meV. For $|\hbar\omega| \sim 1$ meV, the time "seen" by the neutron is $\sim 2\pi/\omega = 4\times 10^{12}$ sec, and a free krypton atom travels about one atomic diameter in this time. A significant conclusion which may be drawn from Figs. 8 and 9 is that the discrepancy is small if $q > q_c = 1.8$ Å^{-1}, and we note that $2\pi/q_c$ is approximately the atomic diameter. Thus we conclude that for many-body collisions involving $t < 2\times 10^{12}$ sec, where r is approximately one diameter, the hard-sphere model is reasonably satisfactory. At longer times and greater distances the attractive part of the pair potential and perhaps many-body forces must play an important role. Computer simulation studies with realistic potentials are required to interpret this region.

Finally, we have plotted the scattering law $S(q,\omega)$ as a function of q for $|\hbar\omega| = 3$, 5, and 7 meV and compared these data with the perfect gas in Fig. 10. It is expected that at high energy transfers the interference effects will become weaker and especially at high q the data approach that for the perfect gas. At $|\hbar\omega| = 3$ meV we can still see a clear interference peak, but its position is moved to a higher q than for either $\omega = 0$ or $S(q)$. For $|\hbar\omega| = 5$ and 7 meV the interference effect is weaker and occurs at still higher q. Table II is a summary of this effect. The effect of increasing density is to shift the maxima slightly and to cause greater deviations from the perfect gas in Fig. 10. This figure can be used also to show that the effects of systematic errors in the correction procedures are small. Not only do the data from the wings of the observed spectra lie in a reasonable relationship to the perfect gas, but if there were a significant error the $|\hbar\omega| = 7$ meV curve would exhibit it because its intensity is very small compared to the data of Figs. 8 and 9.

We conclude that neutron inelastic scattering experiments on dense monatomic gases are feasible, that the van Hove scattering law can be explored systematically as a function of density, and that the results are an excellent test for modern kinetic theories.

ACKNOWLEDGMENTS

Two of us (P.A.E. and D.L.) would like to thank the staff of the ILL for their hospitality during the course of this experiment. Dr. J. Dufty, Dr. B. Alder, and Dr. S. Yip are warmly thanked for providing copies of their theoretical hard-sphere data before publication. Dr. Dufty is thanked especially for his resolution-broadened calculations. This program has been supported by the NRC-CNRS exchange agreement, by the Natural Sciences and Engineering Research Council of Canada, by Der Bundesminister für Forschung und Technologie, Federal Republic of Germany, and by the National Science Foundation of the U.S.A.

[1]A. Teitsma and P. A. Egelstaff, Phys. Rev. A 21, 367 (1980).
[2]P. A. Egelstaff, A. Teitsma, and S. S. Wang, Phys. Rev. A 22, 1702 (1980).
[3]T. A. Postol and C. A. Pelizarri, Phys. Rev. A 18, 2321 (1978).
[4]S.-H. Chen, Y. Lefevre, and S. Yip, Phys. Rev. A 8, 3163 (1973).
[5]P. Verkerk, *Neutron Inelastic Scattering* (IAEA, Vienna, 1977), Vol. II, p. 53.
[6]W. S. Howells (unpublished).
[7]J.R.D. Copley, Comput. Phys. Commun. 9, 64 (1975).
[8]J. R. D. Copley, ILL Internal Report No. 78CO 1645, 1978 (unpublished).
[9]P. A. Egelstaff and A. K. Soper, Mol. Phys. 40, 569 (1980).
[10]J. A. Barker, R. O. Watts, J. K. Lee, T. P. Schafer, and Y. T. Lee, J. Chem. Phys. 61, 3081 (1974).
[11]C. Hoheisel, Phys. Rev. A 23, 1998 (1981).
[12]J. L. Yarnell, M. J. Katz, R. G. Wenzel, and S. H. Koenig, Phys. Rev. A 7, 2130 (1973).
[13]S. Yip, W. Alley, and B. Alder, J. Stat. Phys. 27, 201 (1982).
[14]J. W. Dufty, M. J. Lindenfeld, and G. E. Garland Phys. Rev. A 24, 3212 (1981).
[15]L. Groome, J. W. Dufty, and M. Lindenfeld, Phys. Rev. A 19, 304 (1979).